Estimating the Feasibility of Probing the Epoch of Reionization with the 21cm-Lyα Cross-Power Spectrum

Prepared for:

Drs. Daniel Jacobs (Director), Judd Bowman, & Alex Van Engelen

Arizona State University

School of Earth and Space Exploration

Prepared By:

Tyler Cox

Arizona State University

School of Earth and Space Exploration

Astrophysics Senior Thesis

December 6$^{\text{th}}$ 2019

Abstract

The blah blah blah

Contents

List of Figures

Acknowledgements

First and foremost, I would like to thank my research advisors, Adam Beardsley and Danny Jacobs.

I would also like to thank my second committee member, Judd Bowman.

I would also like to thank my friends and colleagues, who's endless encouragement and blah helped to. In particular, I would like to thank Shane Bechtel, Lily Whitler.

Most importantly, none of this could have been done without the love and support of my family. To my sister, thank you for keeping me humble. To my Mom and Dad, thank you for all you've done.

1 Introduction

1.1 The Early Universe

Immediately following the Big Bang, the Universe was primarily composed of a hot plasma of fundamental particles. In its early state, it was much too hot and dense to form the atoms that form the complex structures the astronomers observe today. Photons that were emitted during this early period scattered off free particles, leaving the Universe opaque to electromagnetic radiation. This lasted until roughly 400,000 years after the Big Bang, at which time the Universe had expanded and cooled sufficiently for electrons to bind to atomic nuclei forming the first atoms of Hydrogen and Helium. Once formed, photons were able to freely propagate through the intergalactic medium (IGM) as cosmic microwave background radiation.

The Cosmic Microwave Background (CMB) is arguably the best studied cosmological period in the history of the universe. Space-based observatories such as WMAP and Planck have measured the CMB with increasing accuracy giving cosmologists insight to the very first fractions of a second after the Big Bang.

Much of the history of the Universe after $\sim$1 billion years the Big Bang is observable as well. Optical and infrared observatories such as those done with the Hubble Space Telescope (HST) allows astronomers to regularly observe redshift galaxies out to $z \sim 4$, while a number of objects at $z > 7$ have been observed with with gravitational lensing. While some objects have been observed at high redshifts, little is known about the period of cosmological time

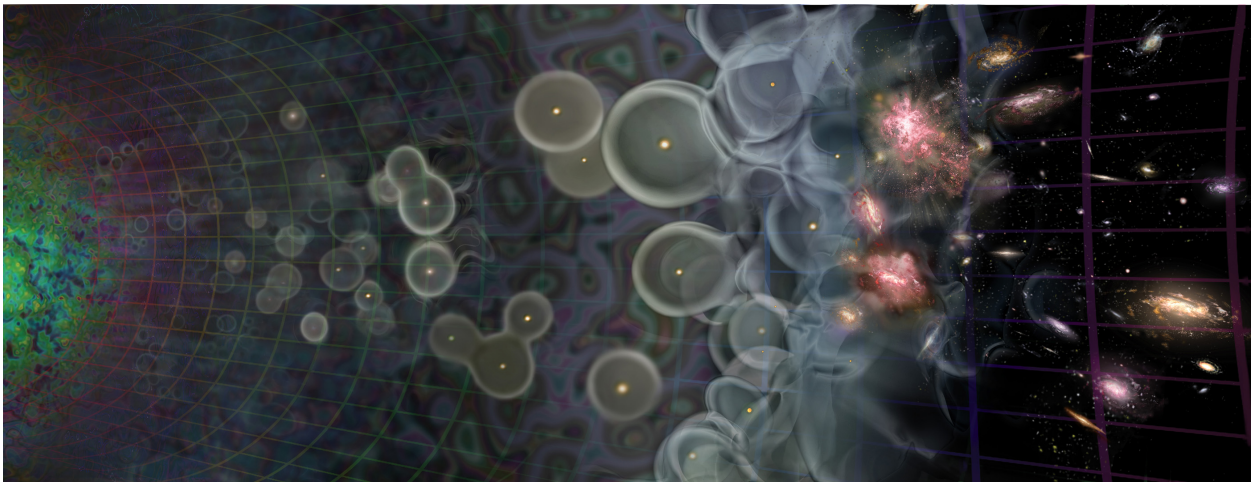

Figure 1. Timeline of the history of the Universe. To the left, is the CMB. To the right, are the stars and galaxies that exist today.

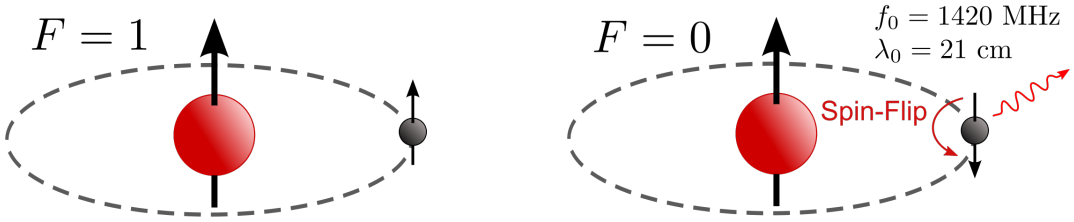

Figure 2. A depiction of the spin flip energy transition of neutral hydrogen. Initially, the spin of the proton and electron are parallel and oriented in the same direction. The energy transition occurs when the electron's spin spontaneously flips from the higher energy parallel alignment to the lower energy anti-parallel alignment, releasing a photon with a wavelength of 21 cm.

between when the.

1.2 The Epoch of Reionization

1.3 Intensity Mapping Experiments

1.3.1 The Hydrogen Epoch of Reionization Array

1.3.2 SPHEREx

SPHEREx looks at things!

2. Modeling 21cm and Lyα Fluctuations

In this section, I will discuss the effort to model the 21cm and Lyα cosmological signals that will be used for cross-correlation later in this work. A significant amount of research has gone into the modeling effort of both 21cm and Lyα fluctuations during the Epoch of Reionization. While N-body and radiative transfer codes and analytic models accurately capture the physics of the evolution of galaxies and the IGM at small scales.

Semi-numerical simulators on the other hand are much more computationally efficient at modeling the large-scale evolution of the IGM throughout the process of reionziation. For this work, I use the semi-numerical simulator of the cosmological 21cm signal, 21cmFAST, to generate the 21cm signal.

2.1. 21cm Fluctuations

In the equation above, T_S is the gas spin temperature, T_γ is the CMB temperature, τ_{ν_0} is the optical depth at 21cm frequency, $\delta_{\rm nl}$ is the non-linear density contrast $\delta_{\rm nl} = \rho/\rho - 1$, $H(z)$ is the Hubble parameter, dv_r/dr is the comoving gradient of the line of sight component of the comoving velocity, where all quantities are evaluated at redshift $z = \nu_0/\nu - 1$.

$$\begin{aligned}\delta T_b(z) &= \frac{T_S - T_\gamma}{1+z}\left(1 - e^{-\tau_{\nu_0}}\right) \\ &\approx 27 x_{\rm HI}(1+\delta_{\rm nl})\left(\frac{H}{dv_r/dv + H}\right)\left(1 - \frac{T_\gamma}{T_S}\right) \\ &\quad \times \left(\frac{1+z}{10}\frac{0.15}{\Omega_{\rm M}h^2}\right)^{1/2}\left(\frac{\Omega_{\rm b}h^2}{0.023}\right)\ {\rm mK}, \end{aligned} \tag{1}$$

In the equation above, T_S is the gas spin temperature, T_γ is the CMB temperature, τ_{ν_0} is the optical depth at 21cm frequency, $\delta_{\rm nl}$ is the non-linear density contrast $\delta_{\rm nl} = \rho/\bar{\rho} - 1$, $H(z)$ is the Hubble parameter, dv_r/dr is the comoving gradient of the line of sight component of the comoving velocity, where all quantities are evaluated at redshift $z = \nu_0/\nu - 1$.

$$\delta_{21}(\mathbf{x}, z) = \frac{\delta T(\mathbf{x}, z)}{\delta \overline{T}(z)} - 1 \tag{2}$$

where $\delta\overline{T}$ is the spatial average of the 21cm brightness temperature offset $\delta T(\mathbf{x}, z)$. Theher

2.2. Lyα Emission

Here we will describe the parameterization of lyman alpha emission during reionization from three dominant sources.

1. Galactic emission
2. Diffuse emission
3. Scattered emission

2.2.1 Galactic

$$L_{\rm rec}^{\rm gal}(M, z) = E_{\rm Ly\alpha} \dot{N}_{\rm Ly\alpha}(M, z) \tag{3}$$

$$f_{\rm exc}(M, z) = f_{\rm Ly\alpha}(1 - f_{\rm esc}(M, z)) A_{\rm He} \tag{4}$$

$$L_{\rm exc}^{\rm gal}(M, z) = f_{\rm exc} E_{\rm exc} \dot{N}_{\rm ion} \tag{5}$$

$$\mathrm{SFR} = 2.8 \times 10^{-28} \left(\frac{M}{M_\odot}\right)^a \left(1 + \frac{M}{c_1}\right)^b \left(1 + \frac{M}{c_2}\right)^d \left[M_\odot \ \mathrm{yr}^{-1}\right] \tag{6}$$

$$I_\nu^{\rm gal}(\mathbf{x}, z) = y(z)\, d_A^2(z)\, \frac{L^{\rm gal}(\mathbf{x}, z)}{4\pi d_L^2} \tag{7}$$

$$\bar{I}_\nu = \int_{M_{\rm min}}^{M_{\rm max}} dM \frac{dn}{dM} I_\nu^{\rm gal}(M, z) \tag{8}$$

2.2.2 Diffuse

$$l_{\rm rec} = E_{\rm Ly\alpha} f_{\rm rec} \dot{n}_{\rm rec}\left(\mathbf{x}, z\right) \tag{9}$$

$$\dot{n}_{\rm rec}\left(\mathbf{x}, z\right) = \alpha_{\rm A} n_e\left(z\right) n_{HII}\left(z\right) \tag{10}$$

This is an equation $n_e = x_i\left(\mathbf{x}, z\right) n_b\left(\mathbf{x}, z\right)$

$$n_b\left(\mathbf{x}, z\right) = \bar{n}_{b,0}\left(1+z\right)^3 \left[1 + \delta_{\rm nl}\left(\mathbf{x}, z\right)\right] \tag{11}$$

$$\alpha_{\rm A} \approx 4.2 \times 10^{-13} \left(T_{\rm K}/10^4{\rm K}\right)^{-0.7} \left(1+z\right)^3 \left[{\rm cm}^3\ {\rm s}^{-1}\right] \tag{12}$$

$$I_{{\rm rec},\nu} = y\left(z\right) d_A^2\left(z\right) \frac{l_{\rm rec}\left(\mathbf{x}, z\right)}{4\pi d_L^2\left(z\right)} \tag{13}$$

2.2.3 Scattered

$$I_\nu = \frac{6 E_{\rm Ly\alpha} d_A^2\left(z\right)}{\left(1+z\right)^2 d_L^2\left(z\right)} J_\alpha\left(\mathbf{x}, z\right) \tag{14}$$

$$\delta I_\nu\left(\mathbf{x}, z\right) = \sum_i \frac{\nu I_{\nu,i}\left(\mathbf{x}, z\right)}{\nu \bar{I}_{\nu,i}\left(z\right)} - 1 \tag{15}$$

3. Cross-Correlation Studies

3.1. Cross-Power Spectrum

$$\langle\widetilde{\delta}(\mathbf{k})\widetilde{\delta}(\mathbf{k}')\rangle = (2\pi)^3\delta_D\left(\mathbf{k}-\mathbf{k}'\right)P(\mathbf{k}) \tag{16}$$

$$\widetilde{\Delta}(k) = \frac{k^3}{2\pi^2 V}P(k) \tag{17}$$

$$\Delta(k) = \left(\nu\bar{I}_\nu\right)^2\widetilde{\Delta}(k) \tag{18}$$

s

3.2. Observational Uncertainties

21cm uncertainty

$$\sigma_{21}^2 = \left[P_{21}\left(k_\perp, k_\parallel\right) + \frac{T_{\rm sys}^2 V_{\rm sur}}{B\ t_{\rm int}\ n(k_\perp)}\right] \tag{19}$$

$$V_{\rm sur} = D^2\Delta D\left(\lambda_{21}^2(z)/A_e\right)^2 \tag{20}$$

Lyα uncertainty

$$P_{N,{\rm Ly}\alpha} = \sigma_{\rm N}^2 V_{\rm vox}{\rm W}_{{\rm Ly}\alpha}(k,\mu) \tag{21}$$

$V_{\rm vox} = A_{\rm pix}r_{\rm pix}$

$$\sigma_{{\rm Ly}\alpha} = \left[P_{{\rm Ly}\alpha}(k,\mu) + P_{N,{\rm Ly}\alpha}\right] \tag{22}$$

21cm-Lyα uncertainty

$$2\sigma_{21,\mathrm{Ly}\alpha}^2 = P_{21,\mathrm{Ly}\alpha}^2 + \sigma_{21}\sigma_{\mathrm{Ly}\alpha} \tag{23}$$

$$\frac{1}{\sigma^2(k)} = \sum_{\mu} \frac{N_{\mathrm{m}}}{\sigma^2(k,\mu)} \tag{24}$$

3.3. Foreground Contamination

$$k_{\parallel} \lesssim \theta \frac{D_M(z)\,E(z)}{D_H(1+z)} k_{\perp} \tag{25}$$

$$\theta = 1.22\frac{\lambda}{D} \tag{26}$$

Here is an explanation of the wedge

Cross correlation of cosmological 21cm observations with Lyα intensity mapping surveys have the advantage that 21cm foregrounds do not correlation with the foregrounds. Because the two do not correlate, no power from the foregrounds is added to the cross-power spectrum. However, while the foregrounds don't contribute to the total cross-power spectrum, they do contribute to the overall variance of the measurement, and therefore the errors.

In the previous section, I calculated the cross-power spectrum for the case where foreground are completely uncorrelated (don't contribute to the cross-power spectrum amplitude) and where they did not contribute to the total variance. In this section, I'll take a more realistic and honest approach to calculating the errors by dealing with the 21cm foregrounds in two different ways. There are two primary methods that I chose to deal with the foregrounds: by relying on the fact that the foregrounds are spectrally smooth and thus confined to an area of the 2D power spectrum known as the wedge and by assuming some imperfect removal method. Each method has advantages and disadvantages.

In addition to avoiding 21cm foregrounds by cutting out k-modes that fall within the wedge, efforts are being made to model 21cm point sources and foregrounds to directly

remove them from the data. This technique is known as foreground subtraction. While this modeling foregrounds accurately has been shown to be quite difficult, it gives the added benefit of recovering the foreground modes that fall within the wedge, increasing the signal to noise of the measurement, assuming perfect (or near perfect) foreground subtraction.

While outside the scope of this particular project, foreground subtraction could be a viable method for recovering k-modes afflicated by bright 21cm foregrounds and potentially allow for higher signal to noise measurements of the cross power spectrum, given sufficient enough subtraction.

I plan to incorporate a treatment of the foreground subtraction in future works. Previous works have handled the modeling of the power spectrum due to bright

$$P_F(q,y) = \sum_j \epsilon_j^2 A_j \left(\frac{l}{2\pi q}\right)^{n_j} \left(\frac{\nu_p}{\nu_i}\right)^{m_j} \tag{27}$$

The total variance on the 21cm-Lyα cross power spectrum measurements would then be written as:

$$2\sigma^2_{21,\mathrm{Ly}\alpha} = P^2_{21,\mathrm{Ly}\alpha} + (P_{21} + P_F + \sigma_{21})\left(P_{\mathrm{Ly}\alpha} + \sigma_{\mathrm{Ly}\alpha}\right) \tag{28}$$

4. Conclusions

This is where my smart words go. I'll say very smart things here. `21cmFAST`

References

Barry, N., Wilensky, M., Trott, C. M., et al. 2019, ApJ, 884, 1, doi: 10.3847/1538-4357/ab40a8

Feng, C., Cooray, A., & Keating, B. 2017, ApJ, 846, 21, doi: 10.3847/1538-4357/aa7ff1

Gong, Y., Silva, M., Cooray, A., & Santos, M. G. 2014, ApJ, 785, 72, doi: 10.1088/0004-637X/785/1/72

Heneka, C., Cooray, A., & Feng, C. 2017, ApJ, 848, 52, doi: 10.3847/1538-4357/aa8eed

Hutter, A., Dayal, P., Müller, V., & Trott, C. M. 2017, ApJ, 836, 176, doi: 10.3847/1538-4357/836/2/176

Kubota, K., Inoue, A. K., Hasegawa, K., & Takahashi, K. 2019, arXiv e-prints, arXiv:1910.02361. https://arxiv.org/abs/1910.02361

Kubota, K., Yoshiura, S., Takahashi, K., et al. 2018, MNRAS, 479, 2754, doi: 10.1093/mnras/sty1471

Mesinger, A., Furlanetto, S., & Cen, R. 2011, MNRAS, 411, 955, doi: 10.1111/j.1365-2966.2010.17731.x

Neben, A. R., Stalder, B., Hewitt, J. N., & Tonry, J. L. 2017, ApJ, 849, 50, doi: 10.3847/1538-4357/aa8f9c

Silva, M. B., & Zaroubi, S. 2018, in IAU Symposium, Vol. 333, Peering towards Cosmic Dawn, ed. V. Jelić & T. van der Hulst, 250–253

Sobacchi, E., Mesinger, A., & Greig, B. 2016, MNRAS, 459, 2741, doi: 10.1093/mnras/stw811

Appendix

This is where appendix-y things go

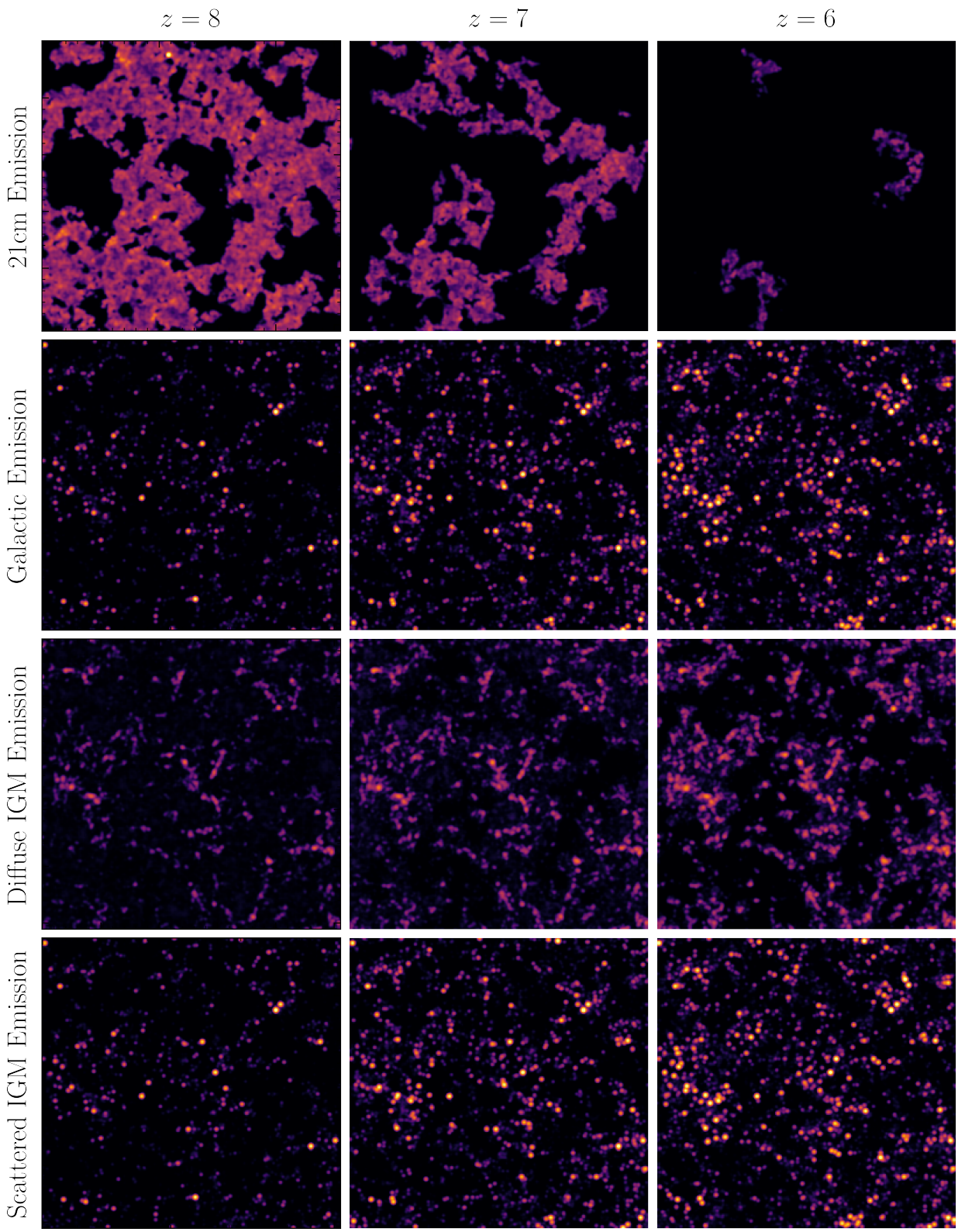

Figure 3. Simulated 21cm and Lyα emission as described in section blah. Each column represents simulated emission at different redshift value.

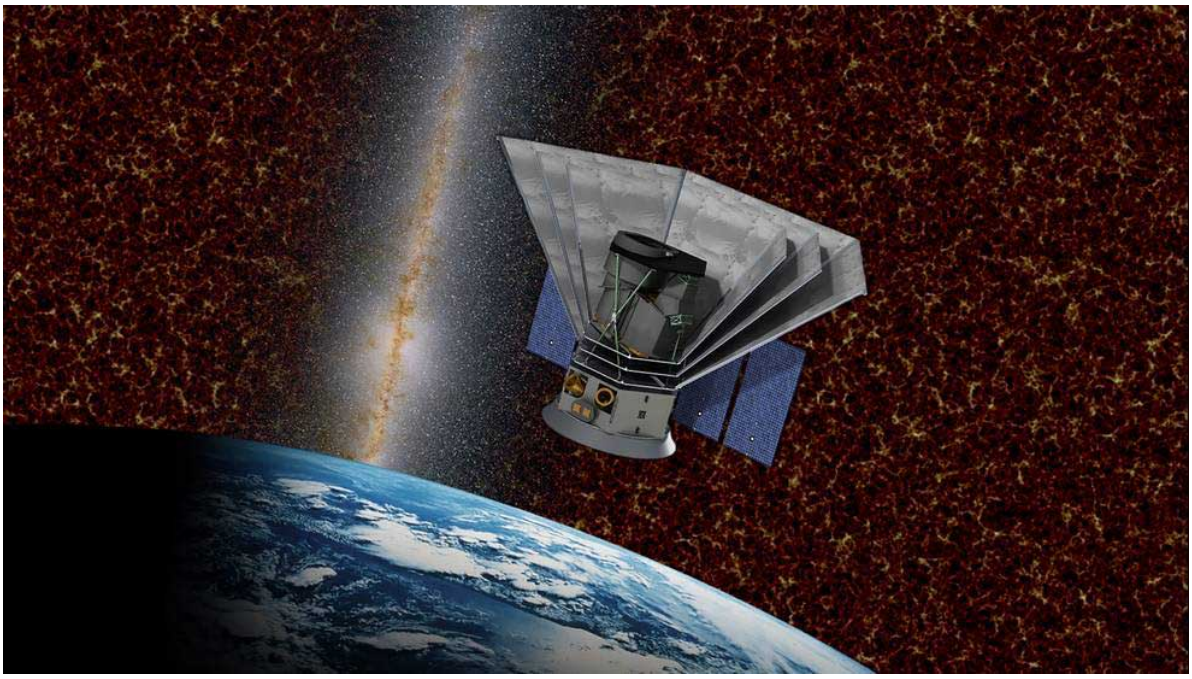

Figure 4. Simulated image of the SPHEREx probe.

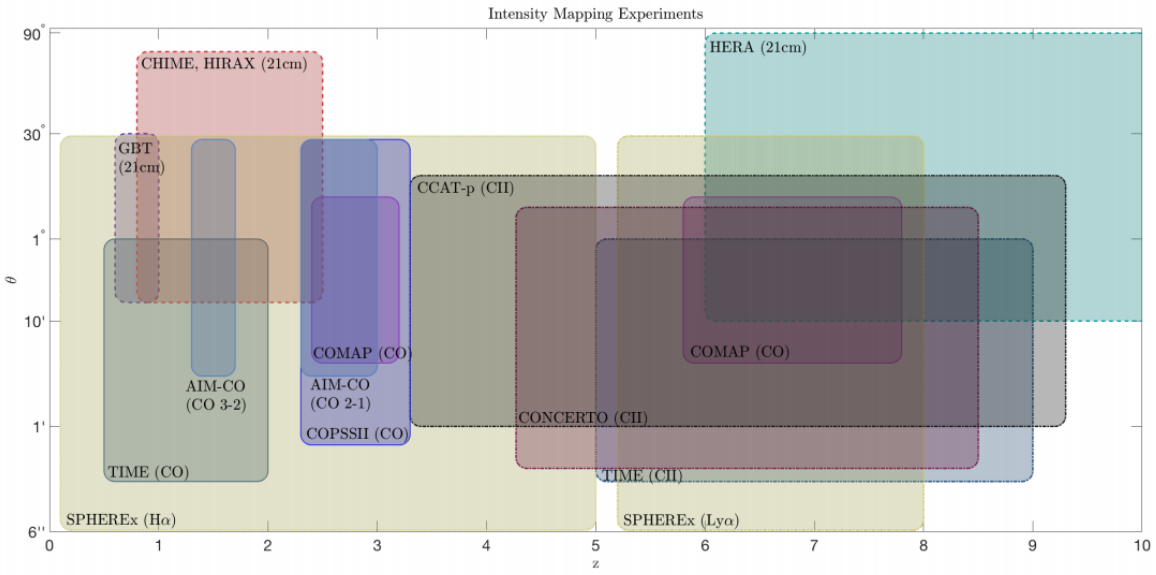

Figure 5

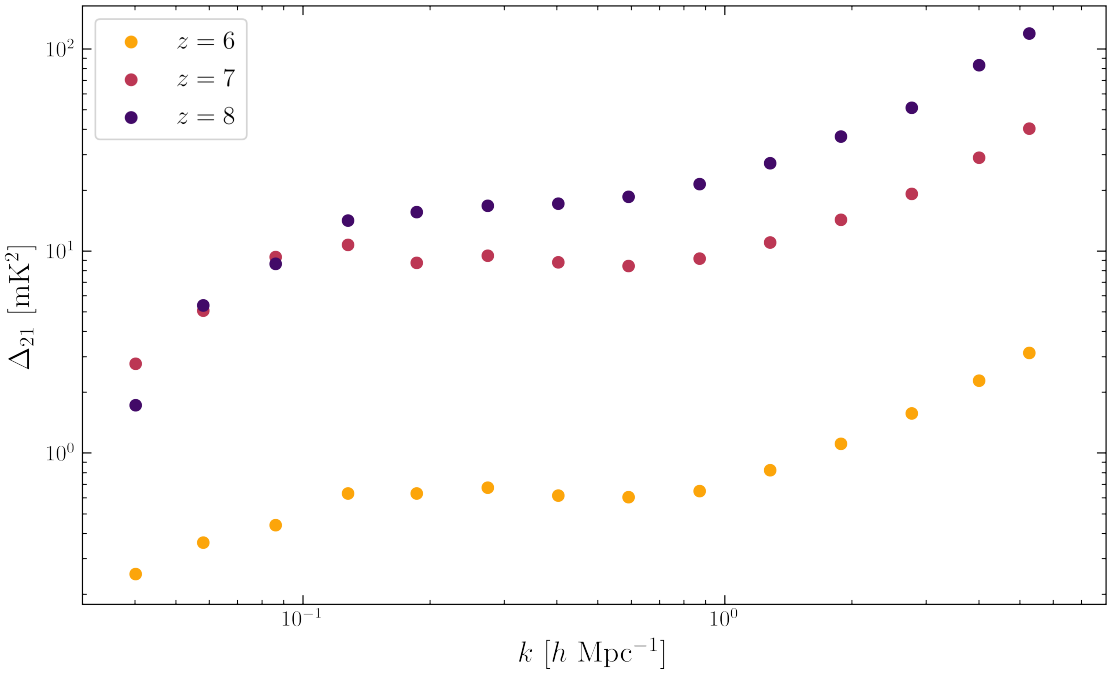

Figure 6. Cross-correlation coefficient

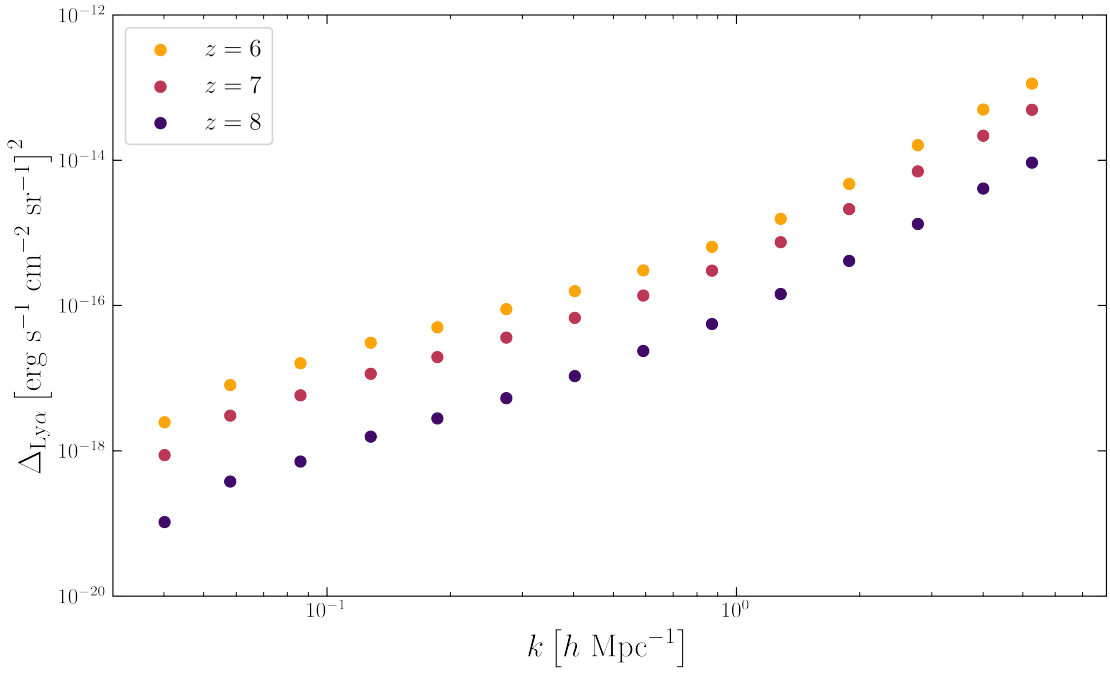

Figure 7. Cross-correlation coefficient

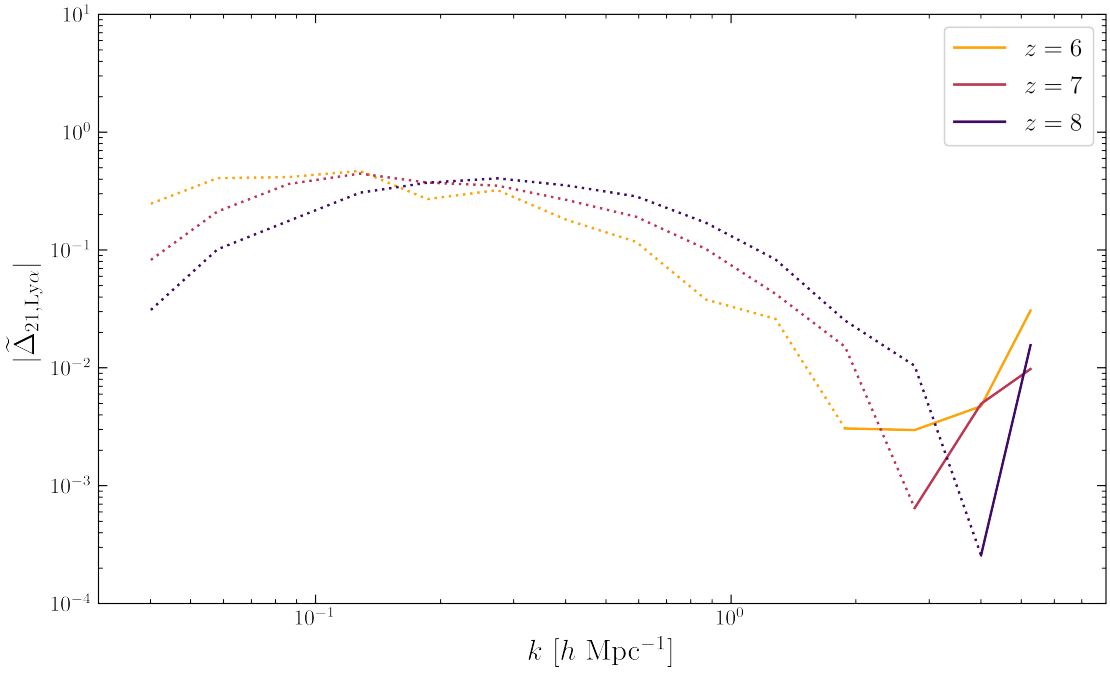

Figure 8. Cross-correlation coefficient

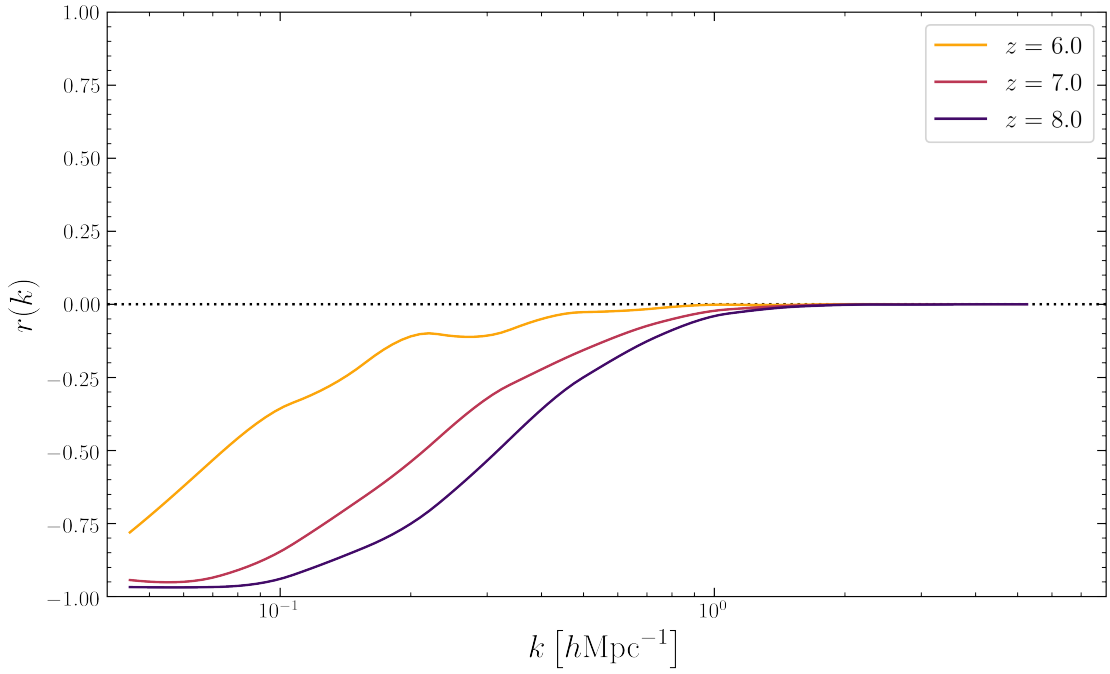

Figure 9. Cross-correlation coefficient

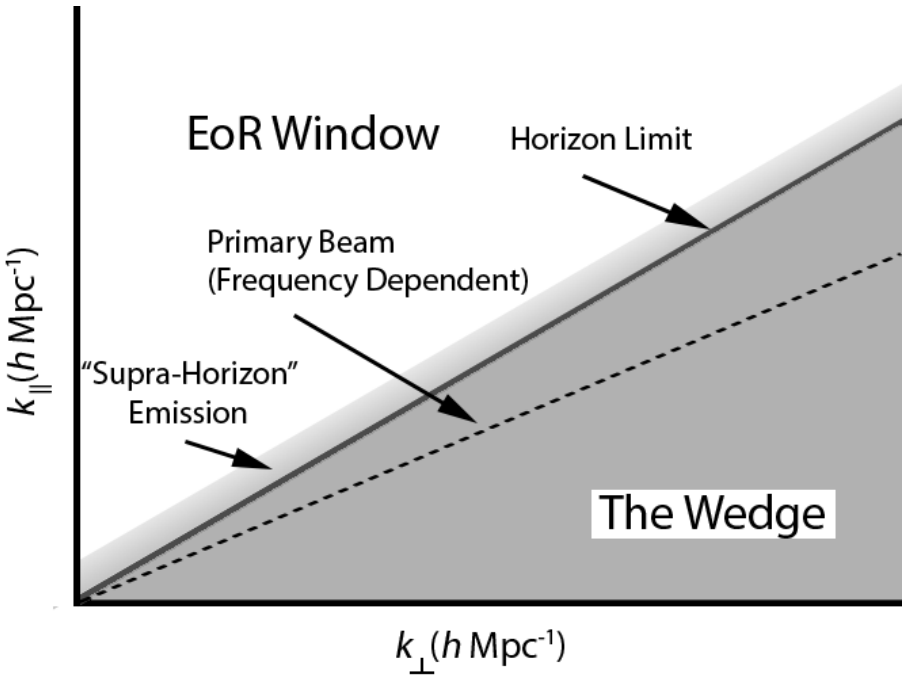

Figure 10. Foreground Wedge

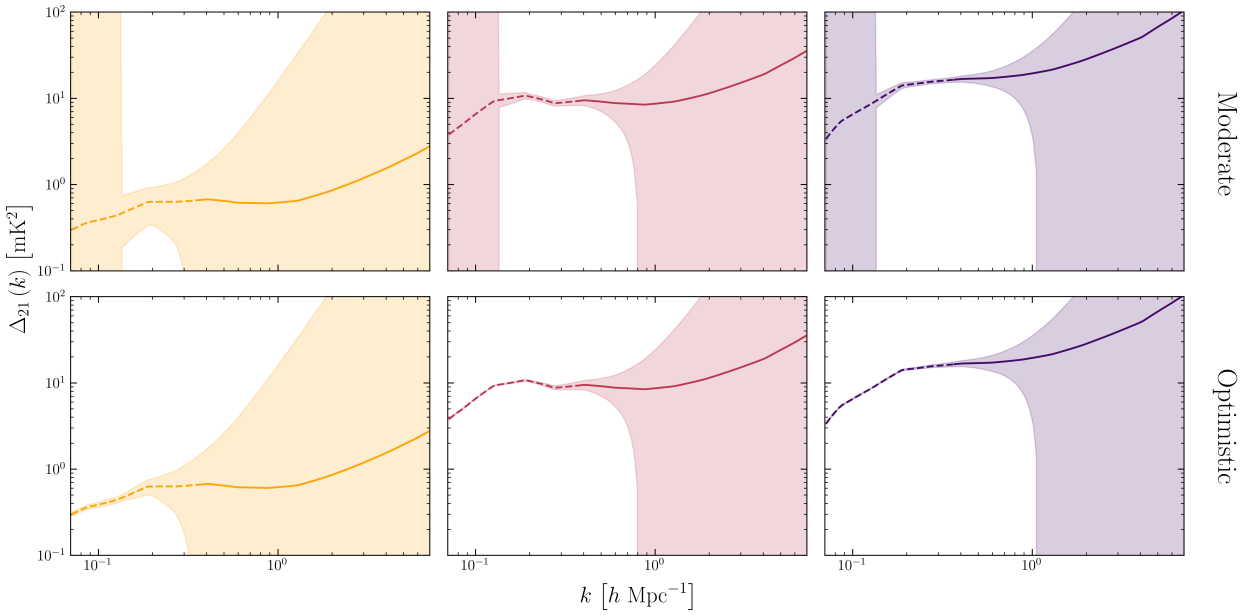

Figure 11. Hello